Biosensors and Bioelectronics 144 (2019) 111679

Contents lists available at ScienceDirect

Biosensors and Bioelectronics

journal homepage: www.elsevier.com/locate/bios

A universal converting strategy based on target-induced DNA nanoprobe conformational change for lead (II) ion assay

Zhehan Yang*, Hong Wu, Xingchen Yi, Jiajia Tang, Wen Yun, Wenbo Han, Xingguang Chen

Chongqing Key Laboratory of Catalysis and Functional Organic Molecules, Engineering Research Center for Waste Oil Recovery, Technology and Equipment of Ministry of Education, College of Environment and Resources, Chongqing Technology and Business University, Chongqing, 400067, China

ARTICLE INFO

Keywords:
Converting strategy
Four-way junction nanostructure probe
Enzyme-free
Pb^{2+}

ABSTRACT

In this work, an electrochemical biosensor combining a novel enzyme-free converting strategy and branched hybridization chain reaction (bHCR) signal amplification for sensitive detection of Pb^{2+} is constructed. Herein, inspired by Holliday junctions nanostructure, a relatively symmetric and stable four-way junction nanostructure probe was prepared by using four DNA stands hybridization including P, S1, S2 and help DNA (hD) with rational design and immobilized onto $Au@Fe_3O_4$ for rapid separation. With unique advantage of nanoprobe, target Pb^{2+} will induce the probe conformational change and release S1, S2 from the $Au@Fe_3O_4$ scaffold to solution, realizing the conversion of input one target Pb^{2+} into two DNA outputs with enzyme-free. To further improve the performance of biosensor, bHCR can be triggered by using S1 and S2 as initiator simultaneously to form reticulated dsDNA nanostructure on the surface of electrode. Then, methylene blue (MB) as electron mediator was embedded into the reticulated dsDNA nanostructure to produce a detection signal. This method introduced a universal converting strategy that molecular unrelated to nucleic acids trigger nucleic acids amplification technology with the help of enzyme-free, which not only widen the application of nucleic acids amplification technology, but also has benefited for molecular analysis.

1. Introduction

Over the past decade, DNA nanotechnology including DNA nanomachines (Ranallo et al., 2017), catalytic circuits (Song et al., 2018), and logic gates (Peng et al., 2018) have been constructed and showed great potential application in gene diagnostic systems, biosensor, molecular imaging (Hu et al., 2019, Ke et al., 2018; Bujold et al., 2018; Wang and Zhang, 2015). Among them, molecular conversion systems based on nucleic acids have an ability to chemically translate any input molecular information into a unique output nucleic acid sequence, which not only extend the generality of sequence-specific nucleic acid detection methods, but also make controlling the operation of dynamic DNA devices by non-nucleic acid targets as a possibility (Srinivas et al., 2017, Beckstead et al., 2016, Lee et al., 2015; Yu et al., 2018). Recently, one general molecular conversion systems based on the target binding-induced DNA strand displacement reaction has been constructed for converting protein, metal ion and small molecular into unique output DNA (Li et al.,2013, 2015; Bai et al., 2014), in which a duplex DNA containing the function strand (aptamer) and output DNA was often chosen as probe, and binding of the probe to the input would induce the release of output DNA, thus resulting in binding-induced DNA assemblies. However, because of the duplex DNA probe itself shortcoming, these systems often suffered from low conversion rates and high background reactivity that can greatly limit their practical applications. Thus, in our previous work, we presented a highly effective protein converting strategy based on immunoreaction-induced DNA strand displacement and T7 Exonuclease (T7 Exo)-assisted protein cyclic enzymatic amplification. With help of T7 Exonuclease, each input protein could induce more than one output single DNA and the conversion rate was greatly enhanced (Yang et al., 2016). Nevertheless, poor stability and the high cost of nuclease hindered the versatility of the applications. From the observations above, we reasoned that the increased conversion rates should be directly combined special structure probes and DNA strand displacement instead of nuclease.

Due to the programmability and biocompatibility of DNA enable the DNA nanostructure with many advantageous such as responsibility to biological cues, ready synthesis, and ease of functionalization place DNA nanostructures, various nanoprobe based on DNA nanostructures including one-dimensional (1D), two-dimensional (2D), and three-dimensional (3D) structures have been designed (Ma et al., 2019; Huang et al., 2018; Cui et al., 2015). For example, Fan group prepared 3D tetrahedral DNA nanostructures as platform for loading affinity ligands

* Corresponding author.
E-mail addresses: yzhzn89@ctbu.edu.cn, yzhan89@126.com (Z. Yang).

https://doi.org/10.1016/j.bios.2019.111679
Received 4 June 2019; Received in revised form 4 September 2019; Accepted 4 September 2019
Available online 07 September 2019
0956-5663/

to well-control densities and orientations of probe (Song et al., 2016). Yuan group designed a 2D DNA nanoprobe (DNP) based on proximity-ligation assay mechanism for improving the efficiency of enzyme-free-target-recycling amplification (Zhang et al., 2018). In light of the above reported work, it is highly possible to rational design and synthesis of DNA nanoarchitectures as nanoprobe to increase conversion rates in conversing strategy. The immobile four-way junction, one kinds of DNA tile, that was built from four single DNA strands, closely resembles the natural Holliday junction, in which strand migration was prevented by minimizing the sequence symmetry in the junction (Hu et al., 2019; Kallenbach and MaSeeman, 1983; Acuna et al., 2012). This nanostructure also was easily collapsed if one of the four strands was displaced by other input, and then release of anther three single stands. Inspired by this mechanism, in this research, we aim to design a novel DNA nanoprobe with better flexibility, stability, and build ability to construct a high efficiency of molecular conversion systems.

In the present work, an electrochemical biosensor combining a novel converting strategy based on four-way junction nanostructure probe, target-induced the probe conformational change and branched hybridization chain reaction (bHCR) (Tang et al., 2017) was constructed for sensitive detection of Pb^{2+}. Firstly, relatively symmetric and stable four-way junction nanostructure probe was prepared by four synthetic DNA strands including P, S1, S2 and hD where P contained Pb^{2+} aptamer. Through our rational design, S1 not only can hybridize to S2, but also has partial same sequences region with S2. Thus, in Pb^{2+} conversion events, S1 and S2 can simultaneously as output DNA to trigger further DNA assembly on the surface of electrode. Secondly, in order to pure the nanoprobe and realize Pb^{2+} conversion, the nanoprobe is immobilized onto the surface of Au@Fe_3O_4 via Au–S bond for further separation. Thirdly, in the presence of Pb^{2+}, the binding of the nanoporbe to Pb^{2+} would lead to the collapse of the nanoprobe, and then S1 and S2 can be released from the scaffold to solution, realizing the conversion of input target Pb^{2+} into output S1 and S2. Importantly, the conversion ratio increased to 1/2 with enzyme-free compared with use of traditional nanoprobe. Subsequently, the solution containing output S1 and S2 then was dropped on the modified electrode to trigger further DNA assembly. The thiol-modified capture hairpin DNA (H1) immobilized onto Au nanoparticles (AuNPs) decorated glassy carbon electrode (GCE). The stem-loop structure of capture probe H1 can be opened by S1 and S2 respectively, and then the complementary sequence of H1 could serve as an initiator to trigger HCR to form dsDNA polymers in the presence of H2 and H3. Similarly, the sequence of subsequent of H2 and H3 would hybridize with H4 and H5 derived by branched HCR. As a result, reticulated dsDNA nanostructure could be formed and then absorbed a large amount of methylene blue (MB), achieving detection signal. Therefore, the sensitivity of the proposed method for detection of Pb^{2+} could be significantly enhanced by using novel converting strategy and bHCR as signal amplification protocol.

2. Experiment section

2.1. Chemicals and biochemical

Au@Fe_3O_4 magnetic nanoparticles were purchased from Shanghai So-Fe Biomedical Co., Ltd. (Shanghai, China). Hexanethiol (HT), MB and gold chloride ($HAuCl_4{\cdot}4H_2O$) were supplied by Sigma (St. Louis, MO, USA). 0.1 M PBS (pH 7.0) containing 0.1 M Na_2HPO_4, 0.1 M NaH_2PO_4 and 0.1 M KCl was used as working buffer solution. TAE buffer (pH 8.0) containing 40 mM Tris-HCl, 20 mM acetic acid, 2 mM EDTA, and 12.5 mM magnesium acetate was used as binding solution.

All synthetic oligonucleotides were ordered from Shanghai Sangon Biological Engineering Technology and Services Co., Ltd. (Shanghai, China), and the sequences were listed Table 1:

2.2. Apparatus and measurements

A conversional three-electrode system including a platinum wire auxiliary electrode, glassy carbon electrode (GCE, $\Phi = 3$ mm) as working electrode and a saturated calomel reference electrode was applied to performed all experiments. Electrochemical measurements including cyclic voltammetry (CV), square wave voltammetry (SWV) and electrochemical impedance spectroscopy (EIS) were carried out on CHI 660E electrochemical workstation (Shanghai Chenhua instrument Co., Ltd, China). CV and EIS experiments were performed in 3.0 mL (5 mM) of $[Fe(CN)_6]^{3-/4-}$ solution with the potential ranging from −0.2 V to 0.6 V. The obtained EIS spectrums were fitted by using ZSimpWin electrochemical impedance modeling software to a modified Randles equivalent circuit. SWV experiments were performed in 3.0 mL (0.1 M) PBS with the potential ranging from −0.5 V to 0 V. Gel electrophoresis was conducted using a DYY-8C electrophoretic apparatus (Beijing, Wo De Life Sciences Instrument Co., Ltd, China).

2.3. Preparation of DNA nanostructure containing Pb^{2+} aptamer probe (nanoprobe)

The DNA nanoprobe was prepared according to the previous method reported in reference with a little modification [Gerling et al., 2015, Wu and Willner, 2016]. Firstly, the four strands including S1, S2, hD, and P, were dissolved in 1 × TAE/Mg^{2+} buffer [40 mM Tris-HCl, 20 mM HAC, 2 mM EDTA, and 12.5 mM Mg^{2+} (pH 8.0)], yielding a final concentration of 20 μM. The resulting mixture was heated to 95 °C for 5 min and then rapidly cooled to 4 °C over 30 s. Secondly, to reduce the signal-noise ratio, Au@Fe_3O_4 was used as scaffold to support the prepared DNA nanoprobe. Briefly, 500 μL of buffer containing 1% (w/w) Au@Fe_3O_4 and 10 μM the prepared thiol-modified DNA nanoprobe was reacted at 4 °C for overnight, and non-hybridized S1, S2 were removed by magnetic force.

2.4. Fabrication procedure of the biosensor for Pb^{2+} detection

The procedure of the biosensor for electrochemical assay of Pb^{2+} is showed in Scheme 1. First, the synthesized DNA nanoprobe incubated with Pb^{2+} samples with various concentrations at 25 °C for 120 min. Then, solutions containing various concentrations of output S1, S2 released from nanoprobe was collected by a magnetic field, and then dropped on the surface of electrode for triggering DNA assembly.

Before using, all the hairpin oligonucleotides solution was warmed to 95 °C for 5 min and then cooling to 25 °C. The electrode was assembled as followed steps: Firstly, A bare GCE was pretreated on the basis of the reported protocol. Secondly, the cleaned GCE was immersed into the solution of $HAuCl_4$ (*w/w*, 1%) and an electrodeposition was conducted at a constant potential of −0.2 V for 30 s to obtain AuNPs layer. Following that, 10 μL of thiol-modified H1 (2.5 μM) was dropped onto the Au/GCE for 16 h at room temperature, leading to assembling H1 on the modified electrode. Subsequently, the electrode surface was blocked with 1.0 mM HT for 30 min. After that, 10 μL of mixture solution containing different concentrations of the released S1, S2 was dropped onto the modified electrode and incubated for 1 h at 37 °C. Then, the electrode incubated with 10 μL of H2 (2.5 μM) and 10 μL of H3 (2.5 μM) at room temperature for 2 h, followed by incubating with 10 μL of H4 (2.5 μM) and 10 μL of H5 (2.5 μM) for 2 h. Ultimately, MB (10 μL, 1.0 mM) as an electron mediator was embed into the dsDNA polymers via electrostatic adsorption.

2.5. Non-denaturing polyacrylamide gel electrophoresis (PAGE)

The notche of the freshly non-denaturing polyacrylamide gel (8%) was used to load the DNA nanoprobe samples and electrophoresis was conducted at 100 V for 30 min in 1 × TBE buffer. The non-denaturing polyacrylamide gel (16%) was used to load HCR samples and

Table 1
List of all DNA sequences employed in this study.

Name	Sequences*(5′→3′)
Probe (P)	SH_2-$(CH_2)_6$-TTTTTACCTGGGTGGGTGGGTGGGT
S1	AAGTGCACT TAATC CCACCCAGGT
S2	GATAAGGGA AGTGCACT TAATCCC
hD	ACCCACCCA CTTAA TCCCTTATC
H1	ACTTAAT CGCCCG GG ATTAAGT GCACTT TTTTT-$(CH_2)_6$-SH_2
H2	CGGGCG ATTAAGT GGCGGG ACTTAAT GGTCAAGAAACC
H3	ACTTAAT CGCCCG ATTAAGT CCCGCC GGTCAAGAAACC
H4	GAAACC CCGCCC GGTTTC TTGACC
H5	GGGCGG GGTTTC GGTCAA GAAACC

electrophoresis was conducted at 120 V for 90 min in 1 × TBE buffer. Before loading, DNA samples were mixed with DNA loading buffer on a volume ratio of 5:1. After separation, the electrophoresis image using the BIO-RAD gel image analysis system (USA).

3. Results and discussion

3.1. Design and optimization of four-way junction nanostructure probe

The principle of Pb^{2+} recognition triggered enzyme-free converting system is illustrated in Scheme 1. The key point of Pb^{2+} conversion is design of DNA nanoprobe, which must meet three requirements: 1) DNA nanostructure should possess strong stability. 2) Binding Pb2+ to DNA nanoprobe can trigger release of more than two single stands DNA from DNA nanoprobe with enzyme-free. 3) The output DNA single stands need to completely open H1 with high efficiency for further DNA assembly. On the basis of Holliday junctions, four synthetic DNA strands are needed to form four-way junction nanostructure probe. Thus, initially, we designed one stand containing Pb^{2+} aptamer and the other three stands have partial same sequences region, which can

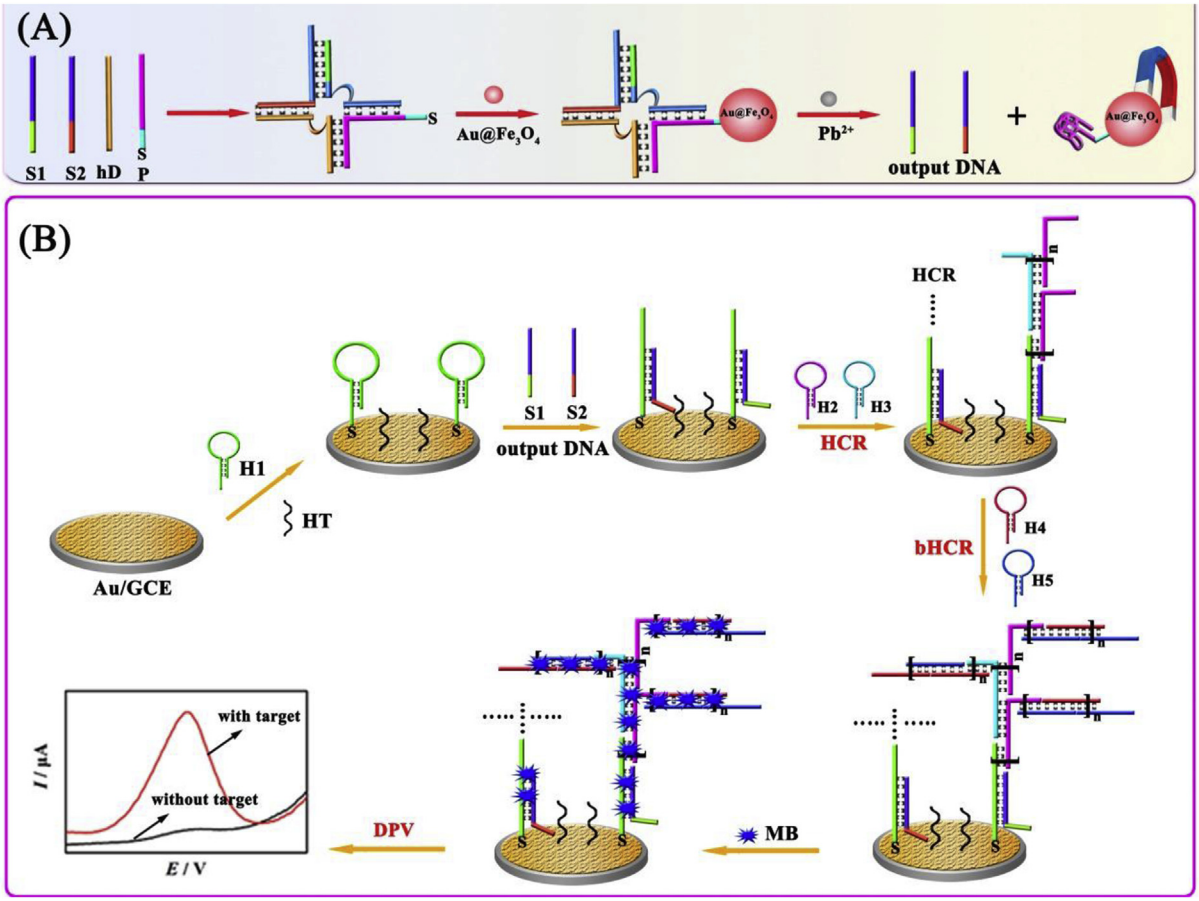

Scheme 1. Converting procedure of Pb^{2+} into output DNA (A), Schematic illustration of electrochemical detection (B).

simultaneously use as output DNA to trigger further DNA assembly on the surface of electrode. However, NUPACK result which can provide the well-studied thermodynamic parameters of nucleic acid hybridization reaction shows that it is hard to maintain balance between the stability and yield of the formed nanoprobe and the efficiency of the output DNA to trigger further DNA assembly. To overcome this disadvatange, a probe DNA (P), a help DNA and two outputs DNA were designed to assemble nanoprobe and the NUPACK result was showed in Fig. S1. It could be seen that the yield is up to 98% and the reaction standard free energy (ΔG) is −57.28 kcal/mol (Fig. S1A). However, when the hybridization reaction occurs among P, S1and S2, the yield is reduced to 29%and ΔG is increased to −38.14 kcal/mol (Fig. S1B), which indicated that hD play an vital role in the formation of nanoprobe. Moreover, the yield of S1 and S2 hybridization with H1 also corresponds to 99% and 97% (Figs. S1C and D). As a result, relatively symmetric and stable four-way junction nanostructure probe was prepared by four synthetic DNA strands including P, S1, S2 and hD where P.

3.2. Morphology of $Au@Fe_3O_4$

$Au@Fe_3O_4$ serves as the scaffold for immobilization of nanoprobe by Au–S bonds in conversion system. Transmission electron micrographs (TEMs) give the size and morphology of the $Au@Fe_3O_4$. The TEM image of the $Au@Fe_3O_4$ was showed in Fig. 1A, it could be seen that the size $Au@Fe_3O_4$ nanoparticles was evenly distributed. From enlarged image in Fig. 1B, a uniform Au shell −3 nm in thickness coated on the surface of Fe_3O_4 core was observed, suggesting that Au shells were successfully grew on the surface of Fe_3O_4. The size distribution in $Au@Fe_3O_4$ nanoparticle suspensions was got accounted. As shown in Fig. 1C, the results revealed that the nanoparticles showed a narrow single peak. The mean diameter (number average) is 43.8 nm and virtually identical to the value for the maximum of the distribution.

3.3. Characterization of biosensor

CV measurements were conducted to characterize the biosensor preparation procedure. As shown in Fig. 1D, curve a showed a pair of well-defined redox peak obtained at bare GCE. When AuNPs were modified electrode, an increase peak current could be observed (curve b) because of conductivity of AuNPs promoted the electron transfer. After H1 was immobilized, a decreased peak current could be observed (curve c). Subsequently, HT was incubated to block the remaining active sites, and peak current further decreased (curve d). When solution containing S1 and S2 was dropped on the modified electrode, the S1 and S2 would hybridize to H1 respectively, which led to the decrease of peak current (curve e). Finally, in the presence of H2 and H3, the complementary sequence of H1 would trigger HCR to form dsDNA polymers. Similarly, the sequence of subsequent of H2 and H3 assembled with the mixture of H4 and H5. As a result, reticulated dsDNA structure which hindered the transmission of electrons was formed on electrode surface, therefore, a decrease peak current could be observed.

To further characterize the modified procedure of the biosensor, the EIS was used to provide additional information. As shown in Fig. 1E, the GCE modified with AuNPs showed a much smaller R_{et} (curve b) than bare GCE (curve a). When H1 incubated to Au/GCE surface, the R_{et} value increased (curve c). When the surface was blocked with HT, the R_{et} value further increased (curve d). After S1 and S2 were dropped, the hybridization events among S1, S2 and H1 led to the increase of R_{et} (curve e). The complementary sequence of H1 then triggered HCR and bHCR in the presence of H2, H3, H4 and H5, the R_{et} was further increased (curve f), which was ascribed to the introduction of more negative charges on the electron surface upon the formation of the reticulated dsDNA polymers. Both CVs and EIS result demonstrated that the biosensor was successfully constructed.

3.4. PAGE analysis

As mention above, the formation of nanoprobe plays an important role in the construction of biosensor. Thus, PAGE (8%) analysis was conducted to characterize the preparation of nanoprobe. As shown in Fig. 2A, the S1, S2, hD and P, exhibited various single band in lanes 1, 2, 3 and 4 respectively. Lane 5 showed the PAGE result for sequential hybridization among the P, S1, S2, and hD at the same concentration of

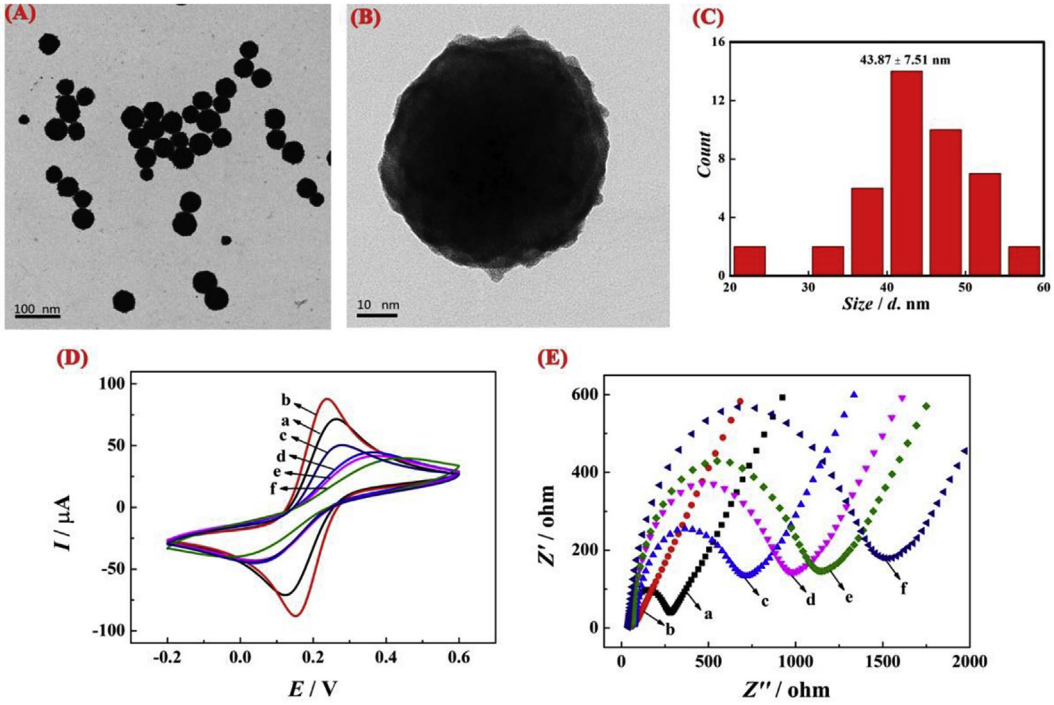

Fig. 1. TEM image(A, B) and size distribution of $Au@Fe_3O_4$ (C), CV(D) and EIS (E) of the stepwise modification processes in $[Fe(CN)_6]^{3-/4-}$: (a) bare GCE, (b) AuNP/GCE, (c) H1/AuNP/GCE, (d) HT/H1/AuNP/GCE, (e) S1/HT//H1/AuNP/GCE (f) H2, H3, H4, H5/S1/HT//H1/AuNP/GCE.

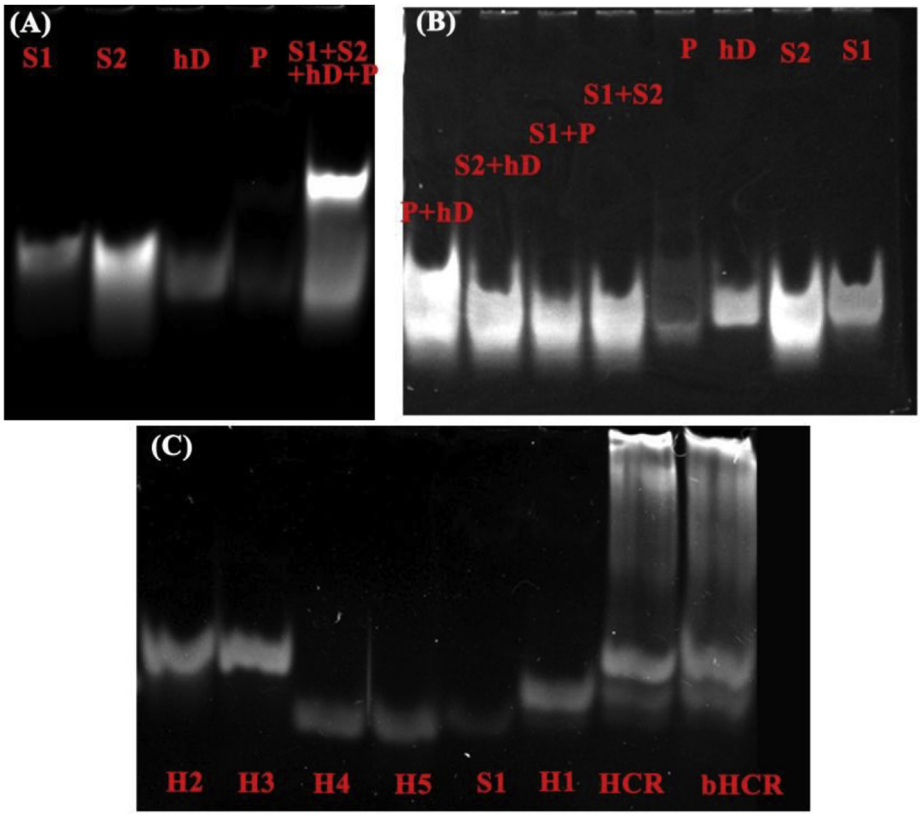

Fig. 2. PAGE analysis of different samples, (A) Line 1: S1; Line2: S2; Line 3: hD; Line 4: P; Line 5: a mixture of S1, S2, hD, and P. (B) Line 1: a mixture of P and hD; Line2: a mixture of S2 and hD; Line 3: a mixture of S1 and P; Line 4: a mixture of S2 and S1; Line 5: P; Line 6: hD; Line 7:S2, Line 8:S1. (C) Line 1: H2; Line2: H3; Line 3:H4; Line 4: H5; Line 5: S1; Line 6: H1; Line 7: a mixture of S1, H1, H2, H3; Line 8: a mixture of S1, H1, H2, H3, H4, H5.

2 μM. As expected, a band with slower mobility could be observed (lane 5 *vs*. 1, 2, 3, 4), indicating successful hybridization among the P, S1, S2, and hD. Additionally, the PAGE results for sequential hybridization between P and hD, between S2 and hD, between S1 and P, and between S2 and S1, were exhibited in Fig. 2B corresponding to lanes 1, 2, 3, 4. All bands in lanes 1, 2, 3, 4 showed almost the same positions in comparison with that of the S1, S2, hD and P in lanes 5, 6, 7and 8, indicating that the hybridizations between two kinds of stands were almost not occurred. This result provided exceptional evidence to demonstrate the successfully preparation of nanoprobe.

Further gel electrophoresis experiments (16%) were performed for S1 trigger-HCR and bHCR. The H2, H3 H4 H5, S1 and H1, in lanes 1, 2, 3, 4 5 and 6 respectively, exhibited a different single band (Fig. 2C). When addition S1 into the mixture solution of H1, H2 and H3 generated a broad band with apparent molecular weights (lane 7), this observation suggested HCR efficient occurrence. After introducing H4 and H5 into above sample, a band with little mobility was obtained (lane 8). This result demonstrated that S1 trigger HCR and bHCR to form the reticulated dsDNA polymers.

3.5. Feasibility of the electrochemical aptasensor for Pb^{2+} assay

To verify the feasibility of the nanoprobe for converting Pb^{2+} into output DNA, binding to nanoprobe with and without Pb^{2+} were investigated. As shown in Fig. 3A, in the absence of Pb^{2+} (curve a), no obvious oxidation peak currents of MB are observed, indicating that the hybridization reaction on the surface cannot be triggered. In contrast, in the presence of 10 nM Pb^{2+}, an obvious oxidation peak current of MB could be observed (curve b), indicating that Pb^{2+} were indeed induced nanoprobe conformation change and then released output DNA to trigger DNA assembly on the surface of GCE. To further verify bHCR for amplification signal, various modified GCE were investigated and conducted by SWV measurements (Fig. 3B). When the HT/H1/Au/GCE was incubated with output S1 and S2, a small oxidation peak current of MB was showed in curve a. After incubation with H2 and H3, an increase peak current could be observed, which was ascribed to that HCR was triggered and dsDNA polymers were formed for immobilizing more amount of immobilized MB (curve b). When H4 and H5 incubated, the peak current further increased, suggesting that designed bHCR could successfully amplify electrochemical signals (curve c).

3.6. Optimization of detection conditions

The experimental parameters including the immobilization concentration of the DNA probes and the bHCR time were optimized to obtain optimal performance of the proposed biosensor. Due to the packing density of the H1 anchored on Au/GCE could intensely influence the analytical performance, the effect of the immobilization concentration of the H1 was investigated by using CV experiments in $[Fe(CN)_6]^{3-/4-}$. As shown in Fig. 3C, it could be seen that the current value of CV gradually decreased with increment immobilization concentration of H1 from 0.5 μM to 5 μM. However, when the concentration of the H1 further increased, there was no significant change of the current value. Such a result indicated that the surface of Au/GCE was saturated with the H1. Therefore, the concentration of the H1 at 5 μM is selected for subsequent experiments.

Because bHCR amplification was triggered by branch sequence of dsDNA polymers from the HCR, steric hindrances and electrostatic repulsion would be limited the bHCR, therefore, the effect of the bHCR time were optimized in this study (Fig. 3D). The proposed biosensor was assessed by using SWV. The incubation time of the bHCR process was examined form 10 min to 150 min as shown in Fig. 5B, The current value increased with the increase of incubation time, and then reached a plateau when it exceeded 120 min, demonstrating that 120 min was enough for bHCR.

3.7. The performance of the biosensor for Pb^{2+} detection

Under optimal conditions, the proposed biosensor was incubated with various concentrations of Pb^{2+} standard solution and performed

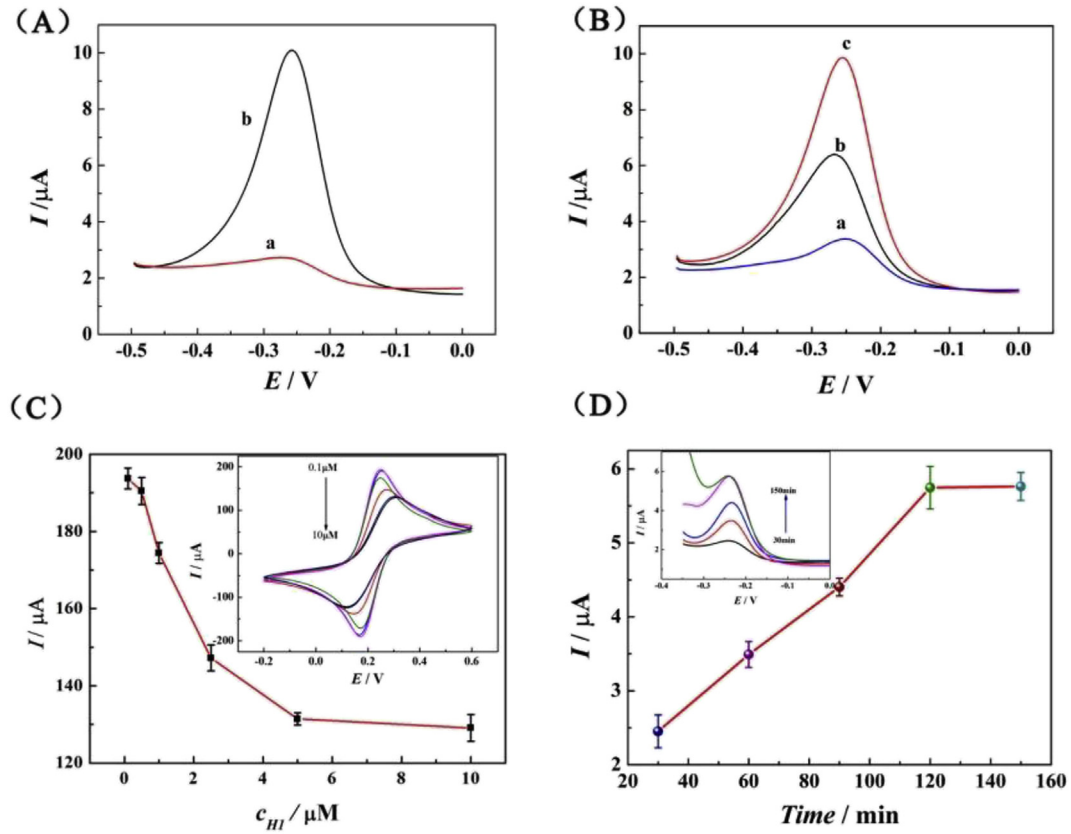

Fig. 3. (A) The SWV response of nanoprobe binding to 0 nM (curve a) and 10 nM Pb^{2+} (curve b); (B) The SWV response of biosensor incubated with output DNA (a), after HCR (b) and bHCR (c). (C) Influence of the concentration of H1 on the biosensor, (D) effect of the time of bHCR on the biosensor.

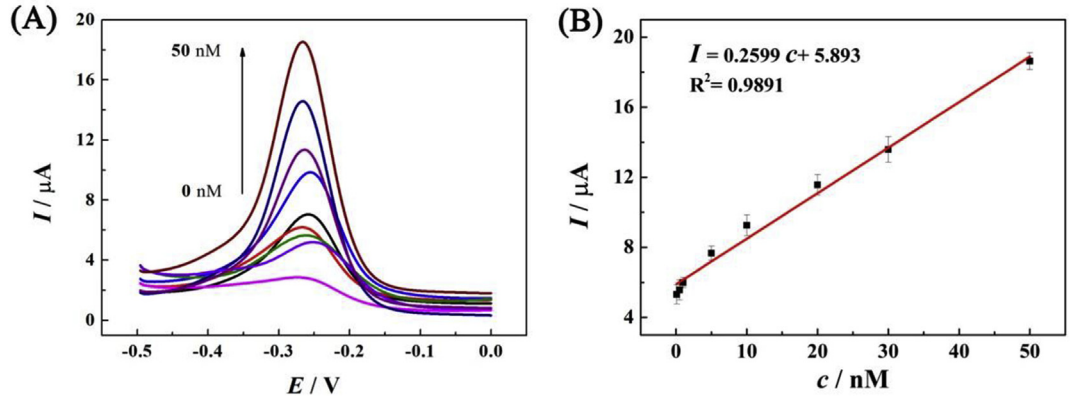

Fig. 4. (A) The SWV response of the proposed biosensor after incubation with various concentrations of Pb^{2+} (A). The calibration plot between the peak currents and the Pb^{2+}concentration (B).

by SWV. As shown in Fig. 4. The peak current of MB increased with increment Pb^{2+} concentration with a linear range from 0.01 nM to 50 nM and the linear regression equation was $I = 0.2599\ c + 5.893$ ($R^2 = 0.9891$) with a detection limit of 8.4 pM (Fig. 4B). The higher sensitivity and wider linear range demonstrated that the bHCR could improve the sensitivity of the biosensor for Pb^{2+} detection. The performance was also compared with some reported methods for Pb^{2+} assay, which indicated that the detection sensitivity was acceptable and competitive (Table 2).

3.8. Selectivity and stability

To challenged the selectivity of the proposed biosensor for the Pb^{2+} detection, Cu^{2+}, Hg^{2+}, Zn^{2+}, Mg^{2+} and Ca^{2+} as possible interferences were estimated under the same experimental conditions to evaluate the selectivity of the biosensor. Compared with the blank test, there were almost no difference of SWV response in the detection of Cu^{2+} (500 nM), Hg^{2+} (500 nM), Zn^{2+} (500 nM) and Ca^{2+} (500 nM) shown in Fig. 5A. However, when biosensor incubated with 10 nM Pb^{2+}, high SWV response was achieved. Meanwhile, while 10 nM Pb2+ coexisted with interferences (500 nM) in the buffer, no obvious signal change existed in comparison with the case of only Pb2+. The result indicated the high specificity of this biosensor for Pb2+ assay. Furthermore, successive cyclic scan was investigated to evaluate the stability of the proposed biosensor. It could be seen that although successive cyclic 50 cycles', the peak current still maintain 90% of initial intensity, indicating that the response current had a relatively stable intensity and the biosensor had good stability (Fig. 5B). The results also indicated

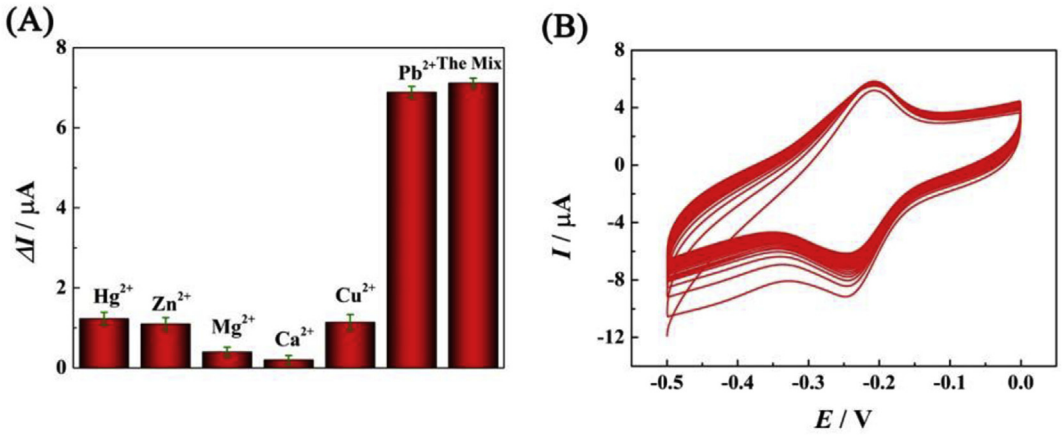

Fig. 5. The specificity (A) and stability (B) of the biosensor.

Table 2
Comparison of the proposed biosensor with other reported methods for Pb^{2+} detection.

Methods	Detection limit	Detection range	References
Fluorescence	50 pM	50 pM–500 pM	Fang et al. (2017)
Surface-enhanced Raman scattering	8.9 pM	10 pM - 1 μM	Shi et al. (2016)
Electrochemistry	0.75 pM	4 pM - 20 nM	Liu et al. (2017)
Electrochemistry	20 pM	30 pM - 1000 nM	Wang et al. (2017)
Electrochemistry	8 pM	10 pM - 1000 nM	Wang et al. (2018)
Electrochemistry	8.4 pM	10pM - 50 nM	This work

that the reticulated dsDNA polymers intercalated with MB maintained favorable electrochemical activity for Pb^{2+}analysis.

4. Conclusion

In summary, we have developed a new and universal translating strategy for electrochemical detection of Pb^{2+} based on four-way junction nanostructure probe, target-induced the probe conformational change and bHCR signal amplification. Because of the special structure of nanoporbe, each input Pb^{2+} could induce two output single strands DNA with enzyme-free, which not only enhance converting ratio but also avoid the disadvantages of enzyme-assisted translating strategy. Additionally, with enzyme-free converting strategy, this method introduced molecular unrelated to nucleic acids to trigger nucleic acids amplification technology which might widen the application of nucleic acids amplification technology and DNA devices. Because of aptamer specific recognition of target Pb^{2+}, it was possible to extend this translating strategy to detection various target including proteins, small molecular and metal ion.

CRediT authorship contribution statement

Zhehan Yang: Conceptualization, Investigation, Formal analysis, Methodology, Writing - original draft. **Hong Wu:** Formal analysis, Writing - original draft. **Xingchen Yi:** Formal analysis. **Jiajia Tang:** Formal analysis. **Wen Yun:** Data curation. **Wenbo Han:** Validation, Visualization. **Xingguang Chen:** Conceptualization, Investigation, Formal analysis, Methodology.

Declaration of competing interest

The authors declare that they have no known competing financial interests or personal relationships that could have appeared to influence the work reported in this paper.

Acknowledgements

The authors are grateful for the National Natural Science Foundation of China (21804014), Chongqing Science and Technology Bureau (cstc2018jcyjA3529), China.

Appendix A. Supplementary data

Supplementary data to this article can be found online at https://doi.org/10.1016/j.bios.2019.111679.

References

Acuna, G., Möller, F., Holzmeister, P., Beater, S., Lalkens, B., Tinnefeld, P., 2012. Science 338, 506–510.
Bai, L., Chai, Y., Pu, X., Yuan, R., 2014. Nanoscale 6, 2902–2908.
Beckstead, A.A., Zhang, Y., de Vries, M.S., Kohler, B., 2016. Phys. Chem. Chem. Phys. 18, 24228–24238.
Bujold, K.E., Lacroix, A., Sleiman, H.F., 2018. Chem 4, 1–27.
Cui, L., Wu, J., Li, J., Ju, H.X., 2015. Anal. Chem. 87, 10635–10641.
Fang, X.N., Liu, Y., Jimenez, L., Duan, Y.K., Adkins, G.B., Qiao, L., Liu, B.H., Zhong, W.W., 2017. Anal. Chem. 89, 11758–11764.
Gerling, T., Wagenbauer, K.F., Neuner, A.M., Dietz, H., 2015. Science 347, 1446–1452.
Hu, Q.Q., Li, H., Wang, L., Gu, H., Fan, C.H., 2019. Chem. Rev. 119, 6459–6506.
Huang, R., He, N., Li, Z., 2018. Biosens. Bioelectron. 109, 27–34.
Kallenbach, N.R., Ma, R.I., Seeman, N.C., 1983. Nature 305, 829–831.
Ke, Y., Castro, C., Choi, J.H., 2018. Annu. Rev. Biomed. Eng. 20, 377–403.
Lee, M.H., Kim, J.S., Sessler, J.L., 2015. Chem. Soc. Rev. 44, 4185–4191.
Li, F., Zhang, H., Wang, Z., Li, X., Li, X.F., Le, X.C., 2013. J. Am. Chem. Soc. 135, 2443–2446.
Li, F., Zhang, H., Wang, Z., Newbigging, A.M., Reid, M.S., Li, X.F., Le, X.C., 2015. Anal. Chem. 87, 274–292.
Liu, F.M., Zhang, Y., Yin, W., Hou, C.J., Huo, D.Q., He, B., Qian, L.L., Fa, H.B., 2017. Sens. Actuators B 242, 889–896.
Ma, J., Xue, L., Zhang, M., Li, C., Xiang, Y., Liu, P., Li, G., 2019. Biosens. Bioelectron. 127, 194–199.
Peng, R., Zheng, X., Lyu, Y., Xu, L., Zhang, X., Ke, G., Liu, Q., You, C., Huan, S., Tan, W.H., 2018. J. Am. Chem. Soc. 140, 9793–9796.
Ranallo, S., Prévost-Tremblay, C., Idili, A., Vallée-Bélisle, A., Ricci, F., 2017. Nat. Commun. 8, 15150–15158.
Shi, Y., Wang, H.Y., Jiang, X.X., Sun, B., Song, B., Su, Y.Y., He, Y., 2016. Anal. Chem. 88, 3723–3729.
Srinivas, N., Parkin, J., Seelig, G., Winfree, E., Soloveichik, D., 2017. Science 358, 1–9.
Song, P., Li, M., Shen, J., Pei, H., Chao, J., Su, S., Aldalbahi, A., Wang, L., Shi, J., Song, S.,

Wang, L., Fan, C., Zuo, X., 2016. Anal. Chem. 88, 8043–8049.
Song, T., Gopalkrishnan, N., Eshra, A., Garg, S., Mokhtar, R., Harish, B., Chandran, H., Reif, J., 2018. ACS Nano 12, 11689–11697.
Tang, Y., Zhang, X.L., Tang, L.J., Yu, R.Q., Jiang, J.H., 2017. Anal. Chem. 89, 3445–3451.
Wang, L.L., Wen, Y.L., Li, L.Y., Yang, X., Jia, N.Q., Li, W., Meng, J.R., Duan, M.L., Sun, X.G., Liu, G., 2018. Biosens. Bioelectron. 115, 91–96.
Wang, X., Yang, C.L., Zhu, S.J., Yan, M., Ge, S.G., Yu, J.H., 2017. Biosens. Bioelectron. 87, 108–111.
Wang, J.S., Zhang, D.Y., 2015. Nat. Chem. 7, 545–553.
Wu, N., Willner, I., 2016. Nano Lett. 16, 6650–6655.
Yang, Z.H., Zhuo, Y.R., Yuan, Y.Q., Chai, 2016. Anal. Chem. 88, 5189–5196.
Yu, Y.J., Yu, C., Niu, Y.Z., Chen, J., Zhao, Y.L., Zhang, Y.C., Gao, R.F., He, J.L., 2018. Biosens. Bioelectron. 101, 297–303.
Zhang, X., Yang, Z., Chang, Y., Qing, M., Yuan, R., Chai, Y., 2018. Anal. Chem. 90, 9538–9544.